Triacylglycerol structures and the chocolate fat bloom mechanism

van Mechelen, J.B.

Chapter 1

Introduction

1.1 Fats

Fats are important ingredients in a broad range of food products like chocolate, butter, spreads and shortenings because they determine physical properties like creaminess, melting behavior, mouth feel and spreadability. For different types of products fats with different properties are required. These properties are determined by the main constituents of fats, the triacylglycerols (TAGs), and in particular by the microstructure that is formed when the majority of the TAGs are co-crystallized.

TAGs consist of a glycerol moiety that has been esterified with three fatty acid chains (Fig. 1.1). In Table 1.1 a selection of fatty acid chains is listed with their identification characters. The names of the TAGs are usually denoted by a three character acronym that represents the fatty acid chains attached to the *sn*-1, *sn*-2 and *sn*-3 position of the glycerol moiety, respectively. The long acyl chains of the TAGs in fats can pack in various ways, depending on the precise temperature, and this leads to the existence of various polymorphs. The TAG polymorphs can be grouped into three types with increasing stability: α, β' and β (Malkin & Meara, 1939).

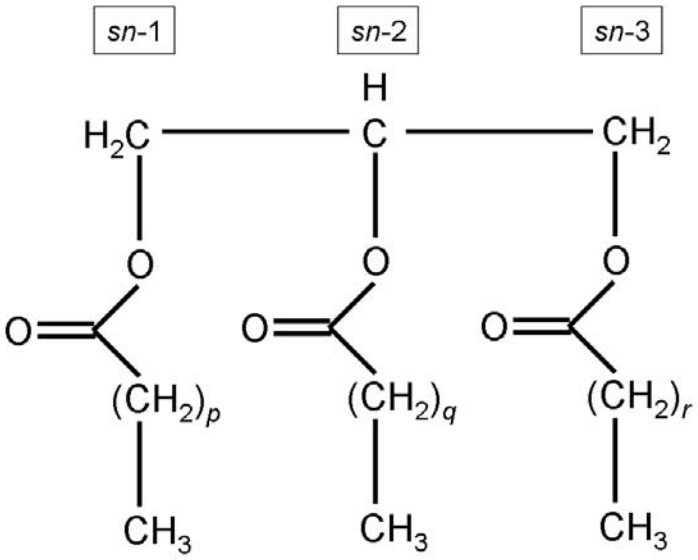

Fig.1.1: Schematic drawing of a triacylglycerol. Acyl chains with a chain length of *p*+2, *q*+2 and *r*+2 C atoms attached to the glycerol moiety at the *sn*-1, *sn*-2 and *sn*-3 position.

Table 1.1: Selected fatty acids

Systematic name	Trivial name	Identifier	Chain length : double bonds
Octanoic	Caprylic	Cy	8:0
Decanoic	Capric	Ca	10:0
Dodecanoic	Lauric	La	12:0
Tertadecanoic	Myristic	M	14:0
Hexadecanoic	Palmitic	P	16:0
Octadecanoic	Stearic	S	18:0
Octadec-*cis*-9-enoic	Oleic	O	18:1
Octadec-*trans*-9-enoic	Elaidic	E	18:1
Icosanoic	Arachidic	A	20:0

The polymorphism of TAGs is monotropic: only one polymorph is stable, either the β' or the β, and a less stable polymorph always transforms into a more stable one (Fig.1.2) (Wille & Lutton, 1966). For β-stable TAGs, the β polymorph is obtained via the β' polymorph and not directly from a seed-free melt. For β'-stable TAGs it is possible to crystallize from a solvent a β polymorph that is less stable than the β' polymorph (Lutton & Hugenberg, 1960). Annealing such a metastable β polymorph close to its melting point will induce a transition to the more stable β' polymorph (see Chapter 5).

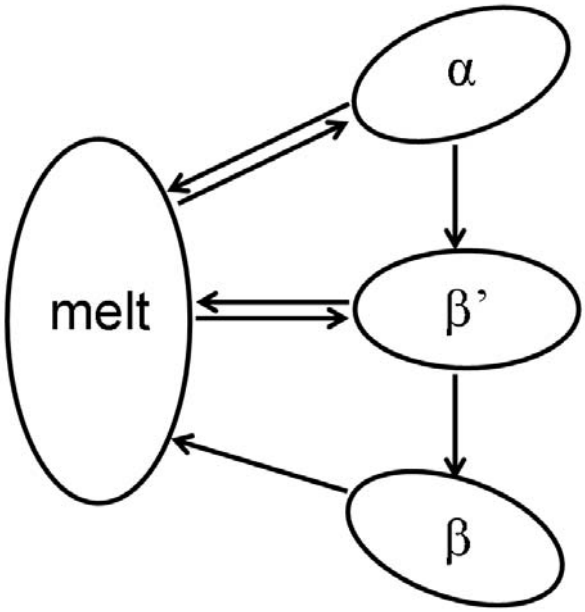

Fig.1.2: Melting and crystallization scheme of TAGs

Natural fats and oils have a high degree of unsaturation. For example, the fat component in chocolate is cocoa butter, a natural fat that contains mainly *cis*-mono-unsaturated TAGs (van Malssen *et al.,* 1996). When these TAGs are co-crystallized in one of the β forms (β-V or β-VI), chocolate gets its appreciated properties that can be expressed as gloss, snap, melting behavior and mouth feel. If chocolate with β-V type cocoa butter is stored improperly (too high temperatures and changes in temperature), the nice gloss of a chocolate bar disappears and is replaced by an undesired whitish layer called fat bloom (Vaeck, 1960). This fat bloom formation is commonly attributed to a transition of the β-V form of cocoa

butter to the β-VI form (Paulicka, 1973). In spite of all efforts, the precise mechanism behind this fat blooming process has not been unraveled up till now. On the basis of the structures presented in Chapters 2 and 3 this mechanism is clarified.

The high degree of unsaturation of natural fats and oils may cause a too high sensitivity to oxidation or a too low melting point. Hydrogenation is used to decrease the tendency to be oxidized and to increase the melting point. However, an undesired side effect of this process is that unsaturated *cis* bonds in the fatty-aid acyl chains can change into *trans* bonds (Grothues, 1985). The resulting so-called *trans* fatty-acid chains are marked as health risks (Oomen *et al.*, 2001), partly because of their assumed similarity in packing compared to fully saturated fatty-acid chains of approximately the same length (*e.g.* E *versus* S or P, Table 1.1) (Björkbom *et al.,* 2007). Verification of these assumptions has not been carried out yet, and little is known about the impact of packing *trans* fatty-acid chains together with fully saturated ones. The β and β' structures presented in Chapters 4 and 5 support most suppositions about the packing similarity between saturated and *trans* mono-unsaturated acyl chains.

X-ray diffraction applied to crystalline material is one of the most efficient techniques to get detailed structural information about the solid-state packing of molecules at the atomic level. Preferably, a single crystal should be grown (**1.2**) and in case of fully saturated TAGs the single-crystal diffraction route has delivered indeed some relevant packing information (**1.3**). However, for mono-unsaturated TAGs this route has never been successful.

Therefore, in this work the focus was on polycrystalline (or powder) material and high-resolution powder diffraction. In particular, new methodology has been used to obtain crystal-structure models from high-resolution powder diffraction data (**1.4**)

1.2 Crystals and diffraction principles

Crystals of organic compounds such as TAGs consist of a three-dimensional periodic packing of (symmetry-related) molecules. Each crystal has a smallest group of atoms from which the crystal can be built by translations only. When this group is represented by a single so-called lattice point, the translation set of lattice points form a lattice. This translation lattice can also be regarded as a stacking of identical unit cells. The unit cell is a parallelepiped that can be described by three vectors **a**, **b** and **c** or, equivalently, by the unit cell axis lengths a, b and c and the interaxial angles α, β and γ. Because of limitations imposed by macroscopic symmetry, each unit cell will belong to one of the seven Bravais lattices (Table 1.2) and if the symmetry elements at the atomic level, and their

combinations, are taken into account as well, the unit cell can be shown to correspond with one of the 230 possible three-dimensional periodic symmetry arrangements called space groups. As a result of the internal symmetry of the unit cell, only the contents of an asymmetric unit has to be described, a symmetry-independent part of the unit cell. The remainder of the cell contents can be generated by applying symmetry operators to this asymmetric unit.

One can envisage a crystal translation lattice being intersected by a family of lattice planes in many ways. Each family consists of numerous parallel planes that all run in an identical way through lattice points and have a constant interplanar spacing, called *d* spacing.

Table 1.2: The seven Bravais lattices

Crystal system	Axis	Interaxial angles
Triclinic	$a \neq b \neq c$	$\alpha \neq \beta \neq \gamma$
Monoclinic	$a \neq b \neq c$	$\alpha = \gamma = 90°$, $\beta \neq 90°$
Orthorhombic	$a \neq b \neq c$	$\alpha = \beta = \gamma = 90°$
Rhombohedral	$a = b = c$	$\alpha = \beta = \gamma \neq 90°$
Hexagonal	$a = b \neq c$	$\alpha = \beta = 90°$ $\gamma = 120°$
Tetragonal	$a = b \neq c$	$\alpha = \beta = \gamma = 90°$
Cubic	$a = b = c$	$\alpha = \beta = \gamma = 90°$

The orientation of a family of lattice planes is defined by its intercepts with the unit cell axes, *a*/*h*, *b*/*k* and *c*/*l*, with *h*, *k* and *l* being integers and relative prime numbers. A family of lattice planes is denoted by the (*hkl*) values or Miller indices and the interplanar spacing as d_{hkl}. An alternative way of representing a family of lattice planes is in the reciprocal space. The reciprocal lattice is described by the vectors $\boldsymbol{a}^*$, $\boldsymbol{b}^*$ and $\boldsymbol{c}^*$ that are normal to $\boldsymbol{b}$ and $\boldsymbol{c}$, $\mathbf{a}$ and $\boldsymbol{c}$, $\boldsymbol{a}$ and $\boldsymbol{b}$, respectively. In the reciprocal lattice the (*hkl*) family of planes is represented by the end point of the vector $\mathbf{H}$,

$$\mathbf{H} = h\mathbf{a}^* + k\mathbf{b}^* + l\mathbf{c}^*$$

The interaction of X-rays with a crystal is an interference phenomenon. When a monochromatic beam of X-rays with wavelength λ has an incident angle θ with a family of planes (*nh nk nl*) (*n* = integer) a positive interference is obtained only when Bragg's law is obeyed:

$$\lambda = 2d_{hkl} \sin\theta$$

This family of planes and the corresponding diffracted intensity are commonly referred to as a reflection with the integer n being the order of the reflection. In practice, one uses the notation (h k l) for reflections, in which the integer h, k and l values are composed from the corresponding Miller indices by multiplying them with the order n of the reflection.

The resultant wave of scattered X-rays, the structure factor, is a function of the ordering of the atoms in the unit cell and can be expressed as:

$$F_{hkl} = \sum_{j=1}^{N} f_j \exp[2\pi i(hx_j + ky_j + hz_j)] = |F_H| \exp(i\varphi_H)$$

in which N is the number of atoms in the unit cell, f_j the atomic scattering factor of atom j and x_j, y_j and z_j its fractional coordinates. The electron density distribution $\rho(x,y,z,)$ in the unit cell is via a Fourier transform related to the F_{hkl} values:

$$\rho(x, y, z) = \frac{1}{V} \sum_{h=-\infty}^{\infty} \sum_{k=-\infty}^{\infty} \sum_{l=-\infty}^{\infty} F_{hkl} \exp[-2\pi i(hx + ky + lz)]$$

For a given θ and (h k l) (= **H**) that fulfil Braggs law, the observable in a diffraction experiment is the intensity I_H. This I_H is proportional to $|F_H|^2$ but the phase φ_H cannot be measured, for none of the reflections, and this poses the so-called crystallographic 'phase problem'. The process of solving this problem is commonly referred to as crystal-structure determination.

A sufficiently large single crystal (Ø = 0.1 - 0.3 mm) can be mounted on a diffractometer head and rotation can bring each (hkl) into a position relative to the incident X-ray beam so that Bragg's law is fulfilled. The amount of reflection intensities that can be measured in this way exceeds by far the amount of atomic positions to be established and crystal-structure determination from such a data set is usually a routine operation.

When the individual crystals are too small to be mounted, powder diffraction is an alternative. The ideal powder diffraction sample consists of many randomly oriented small crystals. Only a fraction of these crystals, those having a lattice plane in an orientation relative to the incident X-ray beam that fulfils Brags law, will contribute to the diffraction signal, an intensity cone around the direction of the incident X-ray beam for each lattice plane (Fig. 1.3). The powder diffraction pattern is the radial intensity profile through the cones perpendicular to the direction of the incident beam. Since half the top angle of this cone equals twice the Bragg angle, this angle (2θ) is taken as the horizontal axis of the powder diffraction pattern.

The breadth (β) of the diffracted intensity peak of a reflection as function of the diffraction angle is inversely related to the size of the crystal (D), as expressed in the Scherrer formula (Klug & Alexander, 1974).

$$\beta = K\lambda / D\cos\theta$$

K is the Scherrer constant, a shape factor that is near unity (Klug & Alexander, 1974). For crystal-structure determination sharp reflections (crystal sizes > 1000 Å) are preferred, but crystals of TAGs are usually smaller so the reflections (*i.e.* the diffracted intensity maxima) are broadened.

In a powder diffraction pattern, the three-dimensional intensity information of the single-crystal experiment is compressed into the single 2θ-dimension, leading to the unavoidable problem of peak overlap.

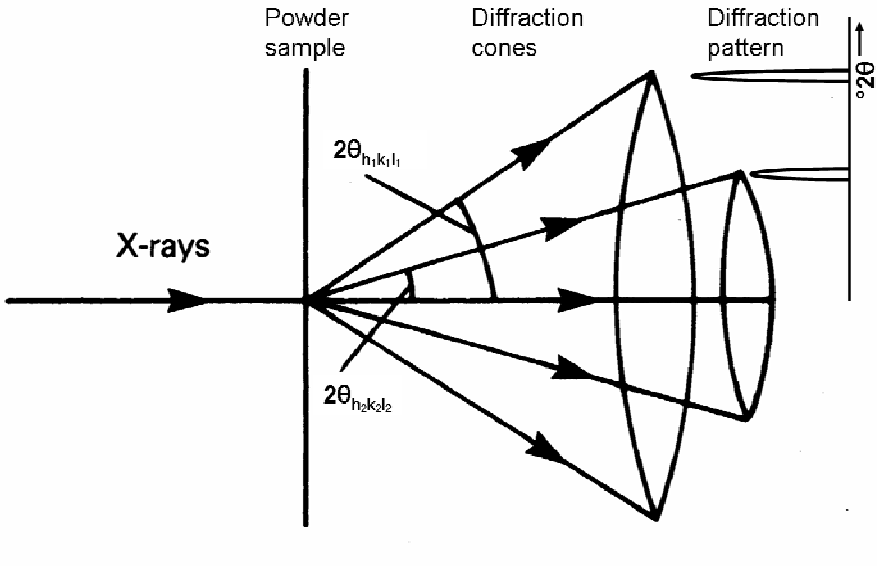

Fig.1.3: X-ray diffraction cones scattered by a powder sample.

1.3 X-ray diffraction of TAGs

The transition of unstable polymorphs into more stable ones may influence the consistency of the fat phase. For a good understanding of the behavior of fats, knowledge of the packing of TAG molecules in the solid state is an important source of information.

From infrared data often a limited characterization of the packing of TAGs can be inferred in terms of the so-called subcell, the smallest repetition unit within the unit cell of the crystal structure along the chain axes (Fig. 1.4) (Yano *et al.*, 1997a,b). The subcell describes the orientation of the zigzag acyl chains relative to each other in the unit cell and contains at least a single ethylene group (de Jong & van Soest, 1978; de Jong *et al.,* 1991). The orientation of zigzags in the subcells commonly reported for TAGs (Fig. 1.5) can be either random relative to the length axes of the chains (α polymorph), alternating parallel and perpendicular (β' polymorph) or all parallel (β polymorph) (Abrahamsson *et al.,* 1978).

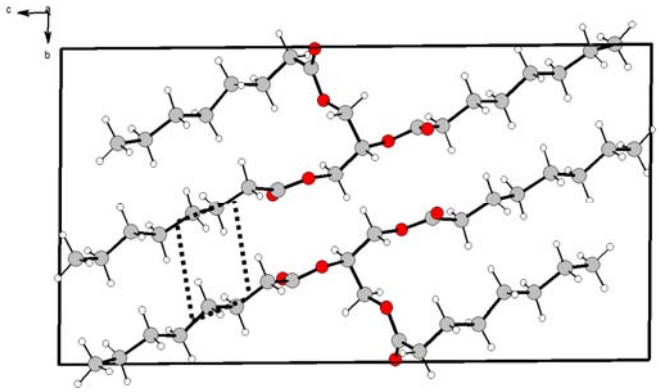

Fig.1.4: View of the triclinic β crystal structure of the TAG CyCyCy (van Mechelen, 2008). The subcell is marked with a dotted line.

From the models available to date, including those discussed in Chapters 2 - 5 of this work, it is clear that TAG molecules tend to pack in a chair-shaped conformation with either a double or a triple chain length packing (Fig. 1.6) (Lutton, 1948).

Each polymorph has characteristic *d* values for long spacings (the low angle peaks that are related to the chain length) and shorter *d* spacings, the so-called finger print lines. Cocoa butter is generally accepted to have five polymorphs (van Malssen *et al.,* 1999). Table 1.2 lists the characteristic *d* values for the five polymorphs of a Brasilian cocoa butter ordered top down with increasing stability.

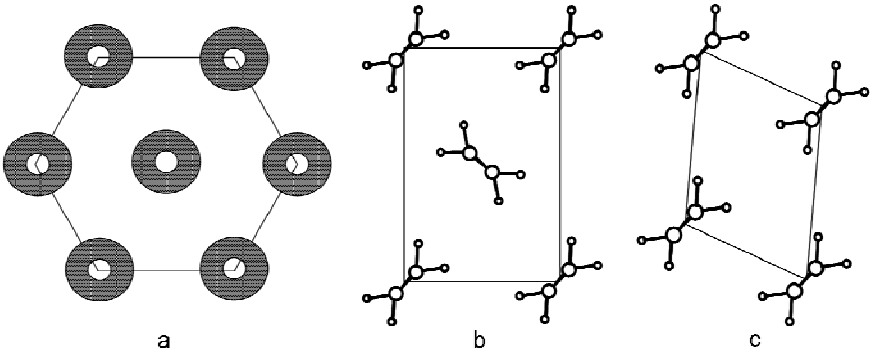

Fig.1.5: Commonly reported subcells of TAG polymorphs. a) hexagonal α subcell; b) orthorhombic β' subcell; c) triclinic β subcell

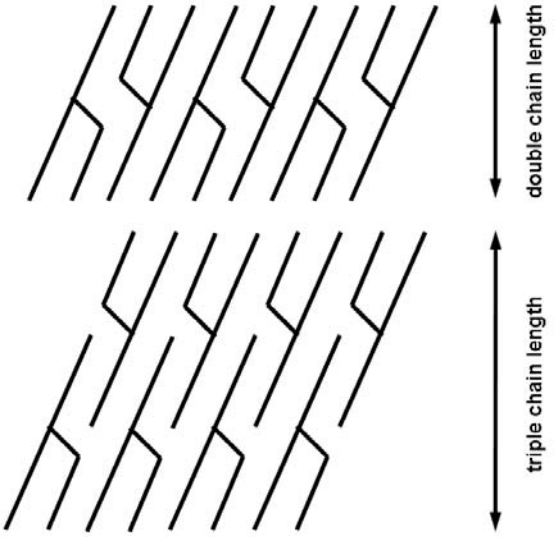

Fig.1.6: Schematic drawing of double and triple chain length packing of TAGs

Table 1.2: *d* values of long spacings and strongest finger print lines of the five polymorphs of a Brazilian cocoa butter and the data collection temperature $T_{data\ coll.}$ (van Mechelen, 2008).

Polymorph	$T_{data\ coll.}$ (K)	Long spacing (Å)	Strong finger print lines (Å)				
γ	267	52.4		4.14	3.69		
α	293	48.4		4.18			
β'	295	45.0		4.33	4.14		
β-V	295	64.8	4.58	3.99	3.87	3.76	3.67
β-VI	295	64.4	4.58	4.03	3.85	3.69	

When TAGs have more than one polymorph of a β or a β' type a numerical subscript is added for a unique identification, the polymorph with the lowest number has the highest stability (*e.g.* β'_1 is more stable than β'_2). A double or triple chain length packing are indicated by addition of '-2' or '-3', respectively. For historical reasons the naming conventions for polymorphs of cocoa butter are different: β-V or form V cocoa butter is equivalent to β_2-3 and β-VI or form VI cocoa butter is equivalent to β_1-3 for pure TAGs (Koyano *et al*., 1990).

The best way to obtain the full packing information is to solve the crystal structure from single-crystal diffraction data. This technique delivers a high ratio of observables (independent reflection intensities) over structural model parameters (atomic coordinates) and results in general fast into an accurate crystal-structure model.

If no suitable single crystal can be grown, as is the case with mono-unsaturated TAGs, the use of powder diffraction data is a possible alternative. The compression of the three-dimensional single-crystal data into the powder diffraction 2θ-dimension causes a loss of independent intensity data. As a result, to solve a crystal structure of even a fairly small molecule (~ 10-20 non-hydrogen atoms) from powder diffraction data was considered quite a challenge.

The structure determination from powder diffraction data was traditionally done by adaptation of single-crystal based techniques, like Direct Methods and Patterson analysis. These techniques require that a sufficient amount of individual reflection intensities can be extracted from the powder pattern in order to be successful, typically for each atom to be located 10 independent reflections need to be available. Moreover, in case of Direct Methods, reflection intensities at atomic resolution (d < 1.6 Å) must be present. In case of mono-unsaturated TAGs both conditions are clearly not fulfilled: the diffraction maxima that can be observed are broad and overlap, especially in the fingerprint area (3-6 Å), while the majority of

TAG polymorphs do not diffract significantly beyond 3 Å so the actual challenge is to obtain a feasible model in spite of having low-resolution data.

In the last decade, significant progress has been made because of the introduction of better diffraction equipment, faster computers and, in particular, the rise of alternative structure determination algorithms, as will be discussed in **1.4.3**.

1.4 Structure determination strategy using powder data

In the process of crystal-structure determination of TAGs using powder data several critical stages can be discerned, (*i*) Sample preparation and data collection (**1.4.1**), (*ii*) Unit cell determination (indexing) and space group assignment (**1.4.2**), (*iii*) Structure determination *i.e.* finding the approximate position and conformation of the molecule(s) in the unit cell (**1.4.3**) and (*iv*) Refinement of the approximate model(s) found in (*iii*) (**1.4.4**).

1.4.1 Sample preparation and data collection

Before a sample is prepared it has to be decided what diffraction instrument and geometry will give the best data set for structure determination purposes. Although a flat sample specimen is relatively easy to prepare, the reflection geometry has several serious disadvantages: preferred orientation is difficult to avoid when preparing a flat sample; sample transparency is high, as TAG samples contain only light elements, and this will broaden and shift the diffraction maxima; the correct sample position is critical as the important low-angle reflections that occur in the TAG patterns are very sensitive to sample height error (displacement error). In this respect the transmission geometry in which a glass capillary is used as sample holder yields higher-resolution data although to fill a capillary with sticky TAG powder can be laborious and longer data collection time is needed.

Preferably, collection of powder data is carried out at a synchrotron source because of the better resolution and much higher photon flux compared to a laboratory powder diffractometer. However, the availability of synchrotron beam time is limited and not available on demand. For the TAG polymorphs we used several powder diffraction stations at the European Synchrotron Radiation Facility (ESRF, Grenoble, France). At the bending-magnet stations BM01b and (the former) BM16 it typically takes 3 to 6 hours to measure a complete high resolution powder pattern. At the insertion device station ID31 a complete data collection is possible in 1 - 2 hours because of the much higher photon flux. This high flux also

allows to crystallize an unstable polymorph "on line" and freezing it when its formation is completed. Disadvantage of the high flux is saturation of the detectors and an increased chance of radiation damage. At ID31 only 2mm of the capillary sample length is exposed to the X-ray beam. At appropriate moments during the data collection the sample (capillary) is moved by 2 mm and fresh material is exposed to the beam, thus limiting the influence of radiation damage.

A second best alternative is using a high-resolution laboratory diffractometer. For our experiments we used two powder diffraction systems, the first is the X'Pert Pro alpha1, a θ-2θ diffractometer equipped with a hybrid monochromator (parallel beam, only Cu $K\alpha_1$ radiation) and an X'celerator solid-state strip detector (both PANalytical, Almelo, The Netherlands). The second system was an X'Pert Pro MPD (PANalytical), a θ-θ diffractometer equipped with an elliptical mirror (high flux convergent beam, Cu $K\alpha$ radiation) and an X'celerator solid-state strip detector. In both systems narrow sollerslits (0.01 rad divergence) have been used to limit axial divergence, the main cause of asymmetry of low-angle peaks. The intensity loss caused by the narrow soller slits was compensated by using the X'celerator strip detector that takes 2° of diffraction data at once. Diffraction data collected with these high-end laboratory diffractometers turned out to be good enough for structure determination of TAG polymorphs as is demonstrated in the work of this thesis.

Control of and cooling to non-ambient sample temperatures is important to prevent radiation damage, especially in case of mono-unsaturated TAGs at ID31, and to grow and stabilize unstable polymorphs in situ. At the ESRF stations the sample temperature was controlled by an Oxford Instruments Cryostream. At BM01b the N_2 stream was perpendicular to the capillary which limited the temperature-controlled sample length to 4mm. At ID31 the capillary sample holder was bathed completely in the N_2 stream, so yielding a constant temperature along the whole length of the sample. The latter type of control was also realized at the X'Pert-Pro systems. Oxford Instruments constructed a shortened model of their Oxford Cryostream that fits inside the enclosure of the X'pert systems.

For a successful structure determination, it is essential that a sample contains only a single TAG polymorph. The presence of an additional polymorph is usually recognized by extra peaks in the low-angle part of the diffraction pattern. An unwanted lower-melting polymorph can be removed by heating the sample just above its melting point. The removal of an unwanted higher-melting polymorph requires a complete melt and subsequent recrystallization. When a polymorph is a stable-end polymorph, annealing close to the melting point may enhance its crystallinity and thus reduce peak overlap.

In our experience, correct intensities of the lowest-angle reflections are essential to obtain a correct structural model. A too conservative beam stop position to avoid detector damage by the primary beam may shield off low-angle diffraction signal and results in too low intensities. This applies to laboratory as well as to the synchrotron systems.

1.4.2 Indexing and space group determination

The starting point for indexing, determination of the unit-cell dimensions, is obtaining accurate peak positions. Generally, a profile fitting program gives the best peak positions. Low angle peaks, however, often have a tail at the low angle side due to axial divergence. This will result in a slightly too low angle of a fitted peak position if the axial divergence is not compensated for.

Indexing is the process that tries to find a unit cell that relates all observed 2θ positions of diffraction maxima to underlying reflections (*hkl*). The relation between the d_{hkl} and the unit cell dimensions is expressed in a form with reciprocal lattice constants (denoted by *) rather than direct lattice constants (Klug & Alexander, 1974):

$$Q_{hkl} = \frac{1}{d_{hkl}^2} = h^2 a^{*2} + k^2 b^{*2} + l^2 c^{*2} + 2hka^* b^* \cos\gamma^* + 2klb^* c^* \cos\alpha^* + 2lhc^* a^* \cos\beta^*$$

Indexing of powder diffraction patterns is usually done with auto-indexing programs. In our experience the popular auto-indexing programs like *Treor* (Werner *et al.*, 1985), *ITO* (Visser, 1969) and *Dicvo*l (Boultif & Louër, 1991), that operate in reciprocal space almost never succeed in indexing patterns of TAG polymorphs because of the (preset) assumptions and fixed settings in the indexing algorithms. Powder diffraction patterns of TAGs are somewhat atypical compared to those of other organic compounds because of the domination by two sets of peaks. In the lower angle part only peaks are found that belong to the same reciprocal lattice line (*d* spacings of ~8 – 65 Å). A second set of overlapping peaks is found at 3.5 – 6 Å, the so-called fingerprint area. To index these atypical diffraction patterns, we developed the real-space indexing routine *LSQDETC* that runs in conjunction with the program suite *POWSIM* (Peschar *et al.*, 2002). *LSQDETC* is a brute-force program that searches through an allowed solution space for cells. The solution space is limited by setting user-definable ranges for the unit-cell parameters and unit-cell volumes, crystal system etc, so prior knowledge (e.g density of the material) can be exploited. From candidate unit cells Q-values are calculated and the cells are ranked according to criteria called Figure of Merit (FOM) that compare the observed set of Q-values with the calculated ones. Commonly used is M_{20}, the De Wolff FOM (de Wolf, 1968, 1972):

$$M_{20} = \frac{Q_{20}}{(2\overline{(Q_{calc} - Q_{obs})} \times N_{20}}$$

Herein N_{20} is the number of calculated Q-values upto Q_{20}. Unit cells with M_{20}>10 are supposed to be serious candidate cells. The correctness of a final indexing is checked with the program *Chekcell* (Laugier & Bochu, 2001). With *LSQDETC* the first powder patterns of monounsaturated TAGs were indexed and based upon this experience later on also patterns could be indexed with the Monte Carlo program *McMaille* (Le Bail, 2004).

In relation to the unit cell also a space group has to be assigned. Unfortunately, the peak overlap in powder diffraction data often obscures the systematic extinctions that result from symmetry elements with fractional translation components (screw axes, glide planes, lattice centering) so an unambiguous discrimination between space groups is not always possible. Moreover, because of the compression into the 2θ dimension acentricity information has been lost. Therefore, the only way to find out the correct space group is to run in parallel structure determinations and refinements for all possible space groups.

1.4.3 Structure determination using direct space global optimization

Since 1998 the influence of the development and availability of global optimization methods is visible in the increasing amount of publications of structures that have been determined from powder data (David & Shankland, 2008). The improved methodology apparently decreased the threshold towards structure solution from powder diffraction data for more complicated crystal structures.

In direct-space methods many trial crystal structures are generated in direct space by changing a small set of structural parameters, like position and orientation of the whole molecule and a selection of torsion angles. For each trial structure a powder pattern is calculated and compared with the observed diffraction pattern. The process of trial-structure generation continues until an acceptable match is found, usually taken as a low-enough *R* factor. The generation of trial structures is done with a Monte Carlo algorithm imbedded in a simulated-annealing approach that slowly decreases the latter temperature of the structure generation. The computation time obviously increases rapidly with the number of structural parameters that is allowed to change, but also the chance to freeze the structure-solution process in one of the many local minima. To prevent getting trapped in a local minimum several optimizations may be run in parallel at different temperatures with regular selection of the most promising one. This so-called parallel tempering process has been implemented in the program *FOX* (Favre-Nicolin & Černý, 2002), one of the most versatile direct-space programs available nowadays.

A *Z*-matrix molecular description is most suited for an efficient molecular description when selection and control of torsion angles is essential. Mean values for bond distances, bond angles and torsion angles were obtained from the CSD. Since the starting model must be and remain realistic, a "randomize starting configuration" option in *FOX*, though helpful for other types of organic compounds, has to be avoided as this makes solving the structure very difficult. Hydrogen (H) atoms are omitted initially in order not to slow down the solution process unnecessarily. The *Z*-matrix description of *FOX* allows for an easy addition of H atoms later on by pasting into the input file.

It should be pointed out that in the course of this work various versions of *FOX* have been used, and that in several instances, upon our request, special alterations were implemented by *FOX* author Dr. Favre-Nicolin to improve the structure-determination process for TAGs. In spite of this additional helpful input, the structure determination of TAGs with *FOX* has turned out to be a laborious process, and far from routine. As the risk of finishing with a wrong structure has to be minimized (Buchsbaum & Schmidt, 2007), continuous inspection of produced models and human intervention including correction of models turned out to be necessary, as will be explained in the Chapters 2-5 in more detail.

1.4.4 Structure refinement

Once an acceptable model has been found, the model has to be refined with a Rietveld refinement program (Rietveld, 1969). Such a program uses a least squares procedure to find the best fit between all the observed intensities I_{oi} collected during a step scan and the calculated profile intensities I_{ci} based on the parameters describing the crystal structure, the diffraction optics, the instrumental factors and other specimen characteristics. The function minimized in the least-squares refinement is:

$$M_p = \sum_i w_i (I_{oi} - I_{ci})^2$$

Herein $w_i = 1/\sigma_i^2$ is the statistical weight of I_{oi}, and I_{ci} the sum of a function describing the angle and (*hkl*) dependant profile of the calculated Bragg intensities and the function describing the background contribution. The number of parameters in the refinement of TAG structures is too large for a stable unrestraint structure refinement. Soft distance and angle restraints have to be applied to

bonding distances, bond angles and soft planar restraints to flat acyl chains to stabilize the refinement. Idealized values for bond angles and bonding distances obtained from the Cambridge Structural Data Base (CSD; Allen, 2002) are used as restraint values. The function M_r to be minimized for the each type of restraint is equivalent to that for M_p:

$$M_r = \sum_j w_j (R_{oj} - R_{cj})^2$$

The weight w_j for each restraint type is decreased during the refinement, but its level is kept high enough to ensure a stable refinement. The sum of the M_r functions is included in the least squares minimization process:

$$M = M_p + \sum M_r$$

The progress of the refinement is monitored by the difference trace of (I_o-I_c). The residuals visualized by this trace are quantified by quality indicators. Two commonly used so called *R* factors are:

$$R_p = \frac{\sum |I_o - I_c|}{\sum I_o}$$

$$R_{wp} = \sqrt{\frac{M_p}{\sum w I_o^2}}$$

Furthermore the χ^2 or Goodness of Fit (GoF or S) is often used as quality indicator.

$$\chi^2 = \frac{M_p}{N_{obs} - N_{\mathrm{var}}}$$

The lower the value of these indicators is the better the quality of the fit and the closer the model of the crystal structure is supposed to approach reality. However, the model of the crystal structure is not the only parameter that determines the lowest reachable level of the R values. Analytical functions that describe the peak profiles and the background should be capable to model the characteristics of the sample and the diffractometer as they appear in the measured diffraction pattern. In single-crystal diffraction, where integrated intensities are used and a profile description does not play a role, R_p values as low as 0.04 are common practice. In powder diffraction R_p values as high as 0.10 are not uncommon, with imperfect description of the diffraction trace as an important reason for the high residue. Rietveld programs offer a choice of profile functions. In most of these functions the Cagliotti function (Cagliotti *et al.*, 1958) is included to model the angle dependant instrumental peak width H:

$$H^2 = U \tan^2\theta + V \tan\theta + W$$

A good profile function for XRPD patterns of TAGs has a mixed Gaussian-Lorentzian function with an asymmetry correction for axial divergence and (hkl) dependant peak-broadening functionality (Finger *et al.*, 1994). For the refinement of the TAG structures discussed in this thesis the program *GSAS* (Larson & Von Dreele, 2000) was used with the graphical user interface *EXPGUI* (Toby, 2001). A Chebyschev polynomial (Abramowitz & Stegun, 1965) was applied to fit the background and profile number 4 to describe the peak profiles. With this function low-angle peak asymmetry and (*hkl*)-dependent broadening can be modeled successfully. All refinable parameters of the profile and background functions, as far as relevant, were part of the refinement process.

1.5 Bibliography

Bish, D.L., & Post, J.E. (1989). *Modern Powder Diffraction*. (The mineralogical Society of America , Washington, D.C.)

Garti, N. & Sato, K. (1988). *Crystallisation and polymorphism of fats and fatty acids.* (Marcel Dekker, New York).

Klug, H.P. & Alexander, L.E., (1974). *X-ray diffraction procedures for polycrystalline and amorphous materials* (John Wiley, New York).

Marangoni, A.G., (2005). *Fat Crystal Networks.* (Marcel Dekker, New York).

Stout, G.H. & Jensen, L.H. (1968). *X-ray structure determination*. (Macmillan Publishing Co. Inc., New York).

Young, R. A. (1997). *The Rietveld Method*, International Union of Crystallography, Oxford University Press, Oxford, England.

1.6 References

Abrahamsson, S., Dahlén, B., Löfgren, H. and Pascher, I. (1978). *Prog. Chem. Fats Lipids* **16**, 125-143.

Abramowitz, M., & Stegun, I.A. (1965). *Handbook of Mathematical Functions*, (New York: Dover), Ch. 22.

Allen, F.H. (2002). *Acta Cryst.* B**58**, 380-388.

Björkbom, A., Ramstedt, B. & Slotte, J.P. (2007). *BBA - Biomembranes* **1768**, 1839-1847.

Boultif, A. & Louër, D. (1991). *J. Appl. Cryst.* **24**, 987-993.

Buchsbaum, C. & Schmidt, M.U. (2007). *Acta Cryst.* B**63**, 926-932.

Cagliotti,G., Paoletti, A. & Ricci, F. P. (1958). *Nucl. Instr*. **3**, 223- 228.

David, W.I.F. & Shankland, K. (2008). *Acta Cryst*. A**64**, 52-64.

Favre-Nicolin, V. & Černý, R. (2002). *J. Appl. Cryst.* **35**, 734-743.

Finger, L.W., Cox, D.E. & Jephcoat, A.P. (1994). *J. Appl. Cryst*. **27**, 892-900.

Grothues, B.G.M. (1985). *J. Am. Oil Chem.* Soc. **62**, 390-399.

Jong, S. de & van Soest, T.C. (1978). *Acta Cryst.* B**34,** 1570-1583.

Jong, S. de, van Soest, T.C. & van Schaick, M.A. (1991). *J. Am. Oil Chem.* Soc. **68**, 371-378.

Koyano, T., Hachiya, I. and Sato, K. (1990). *Foodstructure* **9**, 231-240.

Larson, A. C. & Von Dreele, R. B. (2004). *General Structure Analysis System (GSAS)*, Los Alamos National Laboratory Report LAUR 86-748.

Laugier, J. & Bochu, B. (2001). Chekcell; htp//www.inpg.fr/LMPG.

Le Bail, A. (2004). *Powder Diffr.* **19**, 249-254.

Lutton, E.S. (1948). *J. Am. Chem. Soc.* **70**, 248-254.

Lutton, E.S. & Hugenberg, F.R. (1960). *J. Chem. Eng. Data* **5**, 489-490.

Malkin, T. & Meara, M.L. (1939). *J. Chem. Soc.*, 103-108.

Oomen, C.M., Ocké, C.M., Feskens, E.J.M., van Erp-Baart, M.J., Kok, F.J. & Kromhout D., (2001). *The Lancet* **357**, 746-751.

Malssen, K. van, Peschar, R. & Schenk, H. (1996). *J. Am. Oil Chem.* Soc. **73**, 1217-1223.

Malssen, K.F. van, van Langevelde, A.J., Peschar, R. & Schenk, H. (1999). *J. Am. Oil Chem.* Soc. **76**, 669-676.

Mechelen, J.B. van. (2008). Unpublished data.

Paulicka, F.R. (1973). *Chem. Ind.* **9**, 835-839.

Peschar, R., Etz, A., Jansen, J. & Schenk, H. (2002). *Structure determination from powder diffraction data*, edited by W.I.F. David, K.Shankland, L.B. McCusker, Ch. Baerlocher, (Oxford: Oxford Univ.Press), Chapter 10.

Rietveld, H.M. (1969). *J. Appl. Cryst.* **2**, 65-71.

Toby, B.H. (2001). *J. Appl. Cryst.* **34**, 210-213.

Vaeck, S.V. (1960). *Manufacturing Confectioner* **40**, 35-46, 71-74.

Visser, J.W. (1969). *J. Appl. Cryst.* **2**, 89-95.

Werner, P.-E., Erikson, L. & Westdahl, M. (1985). *J. Appl. Cryst.* **18**, 367-370.

Wille, R.L. & Lutton, E.S. (1966). *J. Am. Oil. Chem. Soc*. **43**, 491-496.

Wolff, P. M. de (1968). J. Appl. Cryst. 1, 108-113.

Wolff, P. M. de (1972). J. Appl. Cryst. 5, 243.

Yano, J., Kaneko, F., Kobayashi, M., & Sato, K. (1997a). *J. Phys. Chem. B* **101**, 8112-8119.

Yano, J., Kaneko, F., Kobayashi, M., Kodali, D.R., Small, D.M. & Sato, K. (1997b). *J. Phys. Chem. B* **101**, 8120-8128.